Climate impacts on patterns of phytoplankton production in Puget Sound, USA: A model synthesis and narrowing of hypotheses

Neil S. Banas, Hoa T.T. Nguyen, Soizic Garnier, Parker MacCready, and Susan E. Allen

November 7, 2019

Abstract

Phytoplankton productivity mediates a wide variety of pathways from regional climate to ecosystem impacts in coastal waters. Results from five recent models of Salish Sea oceanography and regional climate, including both 3D simulations and 1D process models, were synthesized in order to rank and winnow these competing pathways in the Main Basin of Puget Sound, USA. The analysis was organised around four metrics of phytoplankton dynamics that are likely to affect juvenile salmon marine survival and the incidence of Alexandrium harmful algal blooms, both of which have shown alarming trends over recent decades. These metrics consist of annual primary production, date of the spring bloom, phytoplankton concentration during salmon outmigration, and the incidence of strong nutrient limitation in summer.

Results of the multi-model sensitivity and scaling analysis yield relatively simple pictures for climate-linked controls on annual primary production and phytoplankton standing stock, and more complex pictures for bloom timing and summer nutrient limitation, metrics which involve event-scale as well as seasonal-scale dynamics. Overall, results point to incoming light (i.e., variation in cloud cover) as a leading climate influence on Puget Sound phytoplankton dynamics. Variation in riverflow timing, and hence stratification and turbulent mixing, is also likely to drive significant variability and long-term trends in the phytoplankton, as is observed variation in underwater light attenuation. These results suggest a particular research agenda, combining hydrology and watershed processes with the underwater light environment and phytoplankton physiology, as the key to understanding a wide array of climate impacts on the Puget Sound marine ecosystem.

1 Introduction

There are many simultaneous pathways by which regional climate can drive interannual or longer-term variation in primary production in coastal and es-

tuarine waters. Changes in riverflow volume and timing, deep inputs from the open ocean, wind patterns, surface heating, and cloud cover and hence light availability—a partial list—all affect primary production by distinct mechanisms. These climate-linked environmental factors are often highly correlated in historical time series, but may not maintain these correlations into the future as the climate changes; as a result, statistical approaches struggle to identify the specific mechanisms driving historical variability, or the possibly distinct set of mechanisms that will drive future change in marine food webs.

The gold standards in this type of research are long multivariate time series with good spatial coverage (e.g. CalCOFI in Southern California) and coupled hydrodynamic-biogeochemical models driven by regional climate downscalings, well-validated on a range of system levels and scales. These comprehensive datasets generally do not exist, and multi-decadal regional simulations are so cumbersome that even when they do exist, there are invariably system levels at which the key mechanisms have never been directly verified and uncertainty has not been systematically examined. An alternate use of models—which we suggest deserves more articulation and recognition in global change biology—is as a means of *rejecting* hypotheses rather than promoting them: that is, as a means of ranking and winnowing a tangle of competing mechanisms, as a guide for further empirical research.

This study consists of a synthesis of results from hydrodynamically simple (1D) and detailed (3D) models of Puget Sound, USA and the greater Salish Sea, organized around an effort to reduce a conceptual diagram of possible climate-impact pathways from spaghetti (Fig. 1) to a focused research agenda. Primary production affects countless aspects of the marine ecosystem but we have organized our analysis around two larger concerns.

First, chinook, steelhead, and coho salmon runs in the Salish Sea have all experienced tenfold declines in marine survival over the past 30 years (*Zimmerman et al.*, 2015), while chinook and coho on the outer Washington and British Columbia coasts have not shown any matching trend. Active hypotheses that might explain this long-term decline are extremely diverse, encompassing increases in predators, declines in forage fish, changes in physical habitat, chemical pollution, and many other factors; but within this field of inquiry is the fundamental question of whether bottom-up changes beginning at the base of the marine food web could be responsible. Tracing changes in phytoplankton production step-by-step through the long trophic chains that support salmon is well beyond the scope of this study, but with existing oceanographic and earth-system models we are able to begin to evaluate potential past and future trends in *i*) annual primary production and *ii*) the timing of the spring bloom. We also analyze patterns in *iii*) spring and summer phytoplankton concentrations, motivated by a non-trophic hypothesis: the possibility that dense phytoplankton blooms during critical outmigration times change the underwater light field sufficiently to disrupt visual search.

Second, harmful blooms of the dinoflagellate *Alexandrium catenella*, which produces powerful neurotoxins that lead to paralytic shellfish poisoning (PSP), have increased in Puget Sound over the past half-century (*Moore et al.*, 2011).

The seasonal/spatial window of opportunity for *A. catenella* harmful algal blooms (HABs) has been linked to high water temperatures, and this window has expanded over recent decades and is projected to expand further (*Moore et al.*, 2011, 2015). Within the window of opportunity, the occurrence of *Alexandrium* blooms is likely tied to local oceanography via the transport and dispersion of overwintering cysts (*Horner et al.*, 2011)—dynamics that have provided significant predictive ability elsewhere (*McGillicuddy et al.*, 2011)—but also tied to phytoplankton community dynamics and succession. For our purposes, the phenology of the spring bloom (*ii*), as well as *iv*) the occurrence or non-occurrence of strong nutrient limitation in summer, serve as a bridge from Puget Sound oceanography and regional climate to the ecological dimensions of *Alexandrium* HABs, which a lack of detailed, sustained observations has to date left in the realm of speculation (*Moore et al.*, 2015).

Ultimately we would want to evaluate spatial variation in metrics *–iv*) in detail, but for this study we confine ourselves to a typical location in central Main Basin (Fig. 2), insofar as there is any typical location in this complex inland sea.

1.1 Initial conceptual model

Our a-priori conceptual diagram (Fig. 1) does not include every possible route from regional climate to primary production, but rather a pre-selection based on past research in this system (*Winter et al.*, 1975; *Newton and Van Voorhis*, 2002; *Banas et al.*, 2014; *Moore et al.*, 2015). In general, primary production is regulated by light availability (pathway **L**) and nutrient availability (**S**). In addition, temperature (**H**) affects both the maximum growth rate of the phytoplankton community and the rate of losses to micrzooplankton and other grazers. Light limitation is regulated by incoming photosynthetically available radiation (PAR) and hence cloud cover (pathway **A**, **D**); the per-meter underwater light attenuation, which varies strongly with watershed inputs (**B**); and also vertical mixing and advection (**K**, **O**), which control the depth range over which phytoplankton cells are dispersed and hence the light level they experience. Nutrient flux into the euphotic zone is also controlled by vertical mixing and advection (**R**, **R**), and potentially by changes in the concentration of nutrients in incoming ocean water (**T**, **U**). In other estuaries, changes in river-derived nutrients would be of first-order importance as well, but nutrients in Puget Sound are overwhelmingly ocean-derived (*Mackas and Harrison*, 1997; *Mohamedali et al.*, 2011). Watershed-derived nutrients have been found to have notable effects on Puget Sound water quality (*Khangaonkar et al.*, 2019) but these effects are spatially limited (*Banas et al.*, 2014), and the conceptual model and analysis in this study are designed to describe the main stem of Main Basin, away from localised areas of more intense river influence.

Along-channel gradients in nutrients and phytoplankton concentration are relatively weak in Main Basin (*Winter et al.*, 1975, analysis below) and this invites us to consider primary production in a 1-D, single-water-column framework, a modified version of a classic open-ocean scenario. Seasonally varying

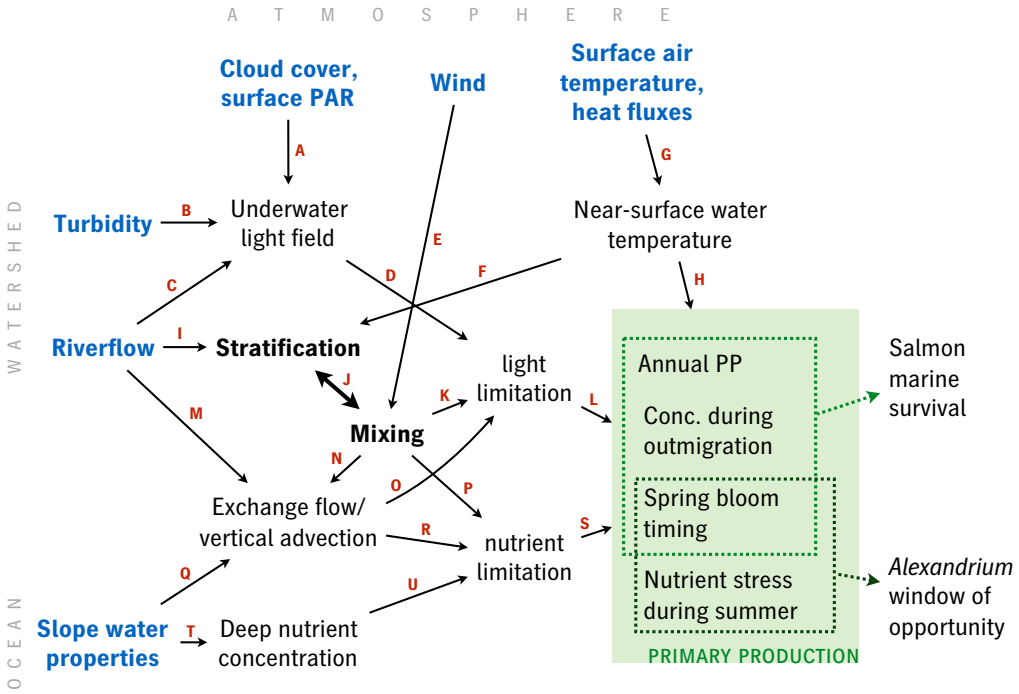

Figure 1: Potential mechanistic pathways from regional climate variability to primary production in the main stem of Puget Sound, away from areas of localized, strong terrestrial influence. Each arrow ($X \longrightarrow Y$) can be read as "Interannual and longer-term variability in X causes interannual variability and longer-term in Y": shorter timescales of variation are not included. Patterns of primary production are represented by four metrics (green shaded box) which have been hypothesized to drive two types of further ecological effects (right). Other pathways of influence on salmon marine survival and *Alexandrium* HABs, e.g. direct temperature effects on *Alexandrium* growth (*Moore et al.*, 2015), are omitted. Compare Fig. 20.

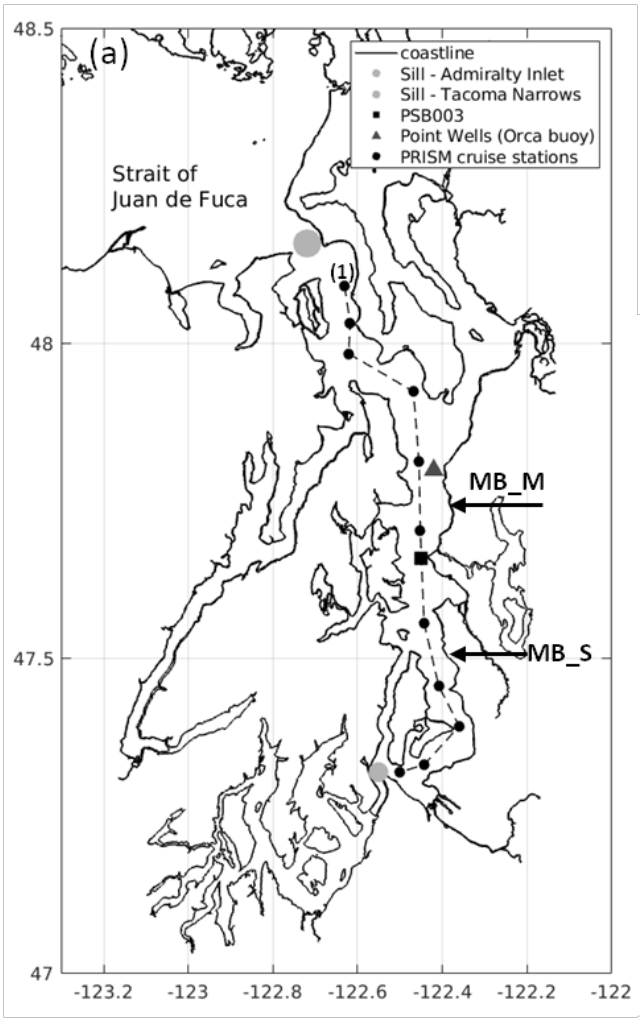

Figure 2: Map of study area. —Washington Department of Ecology (DOE) long-term monitoring station PSB003 (black square), near West Point, is the focus of the analysis.

stratification and mixing are the crucial physical controls on primary production in this classic, mid-latitude framework, with mixing regulating light limitation in early spring (**K**) and hence the timing of bloom initiation, and regulating nutrient availability through the late spring and summer (**P**), once the phytoplankton have drawn down the initial stock of euphotic-zone nutrients left over from winter. Near-surface mixing is driven in part by wind stress (**E**), and in part (in shallow areas especially) by the tides; we have assumed that the tides do not respond significantly to climate change and neglected them in our schematic, which is meant to represent mechanisms of variability and change on annual to decadal scales. The intensity of mixing that results from a given input of wind or tidal energy is strongly regulated by stratification, and conversely stratification records a history of the amount of mixing that has recently occurred (**J**). Since measurements of stratification are far easier and far more common than measurements of turbulent mixing, the literature often elides the distinction and refers to "the effect of stratification on primary production"; but in a highly dynamic, advective environment like an estuary, the distinction between "mixed" water and "mixing" water—that is, low stratification and high turbulent mixing intensity—is potentially very important (*Collins et al.*, 2009; *Franks*, 2015). Riverflow affects estuarine hydrography and energetics through a complex set of feedbacks, but in a first approximation, it drives changes in stratification directly (**I**), and changes in mixing only indirectly (**I** $\rightarrow$ **J**). Surface heating can also affect stratification (**F**), although this effect is usually weaker than river/salinity effects in temperate estuaries.

In Main Basin as in other estuaries, the density contrast between river and ocean inputs drives an "in–up–out" overturning or estuarine circulation (**M**, **N**, **Q**), which regulates the system's overall residence time. The "up" branch of this circulation is the mechanism of mean vertical advection mentioned above, a potentially important contributor to near-surface nutrients (**R**). The inclusion of upward advection reflecting the system-scale circulation and residence time is the crucial addition that turns a generic water-column model into a estuarine water column (*Winter et al.*, 1975; *Collins et al.*, 2009). The along-channel component of the estuarine circulation also needs to be included in tracer budgets if along-channel tracer gradients are large, although we find that for Main Basin chlorophyll and nitrate they are not (Sec. 2.3.1), and care must be taken to preserve mass conservation in tracer budgets in any case.

The aim of this study is to compare the strength of the many interwoven pathways in this conceptual model, in a general, scaling sense rather than a detailed, scenario-specific sense, and produce a simplified conceptual model that eliminates the second-order factors that are overwhelmed by other mechanisms on interannual and longer timescales. This requires associating a *scale of variation* with each atmospheric, watershed, and oceanic driver (Fig. 1, blue), and a *sensitivity* with each mechanistic link (arrows). Estimates of these quantities were assembled from a family of recent model studies that, together, more or less span the timescales and levels of physical and biological process detail required. The results suggest specific research agendas for future oceanographic, atmospheric, and hydrological modelling in Puget Sound and its watershed.

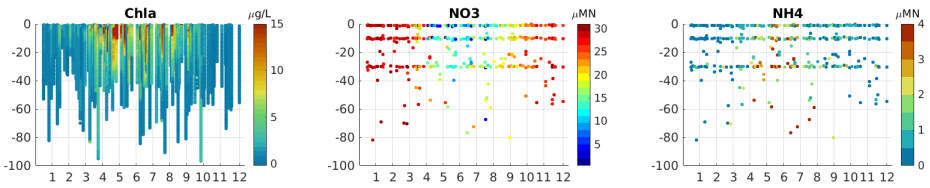

Figure 3: Chlorophyll, nitrate, and ammonium data from Washington Department of Ecology station PSB003 in central Main Basin. Approximately 160 profiles over 17 years for Chlorophyll and 130 profiles over 12 years for nitrate and ammonium are shown.

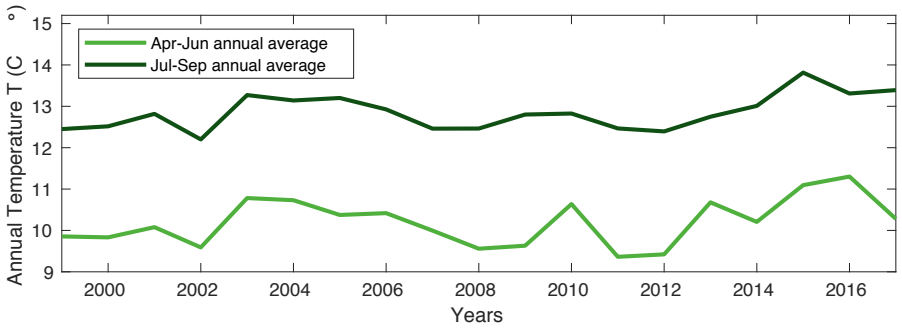

Figure 4: Annual surface temperature from monthly observations 1999–2018 showed averaged for the spring and the summer season.

2 Methods

2.1 Observations

In situ time series Nutrients and biomass Monthly sampling at Washington Department of Ecology (DOE) long-term monitoring station PSB003 provided core time series of temperature, salinity, chlorophyll, nitrate and ammonium at our study site, at approximately monthly resolution. Chlorophyll estimates are from calibrated fluorometer profiles at 0.5 m resolution, while, nitrate and ammonium concentrations are from bottle samples, generally at 1, 10 and 30 meter depth (Fig. 3). In our analysis, near-surface temperature T_{20} is defined as 0–20 m average of approximately monthly observations from PSB003, 1999–2017 (Fig. 4). Density stratification $\delta\rho$ is defined as the difference between 5–20 m average density and 0–5 m average density.

Riverflow Time series of riverflow Q_r (Fig. 5) were derived from USGS gauge data combined with corrections for gauged/ungauged watershed area, as in the setup of the LiveOcean model described below. Q_r is defined as the sum of

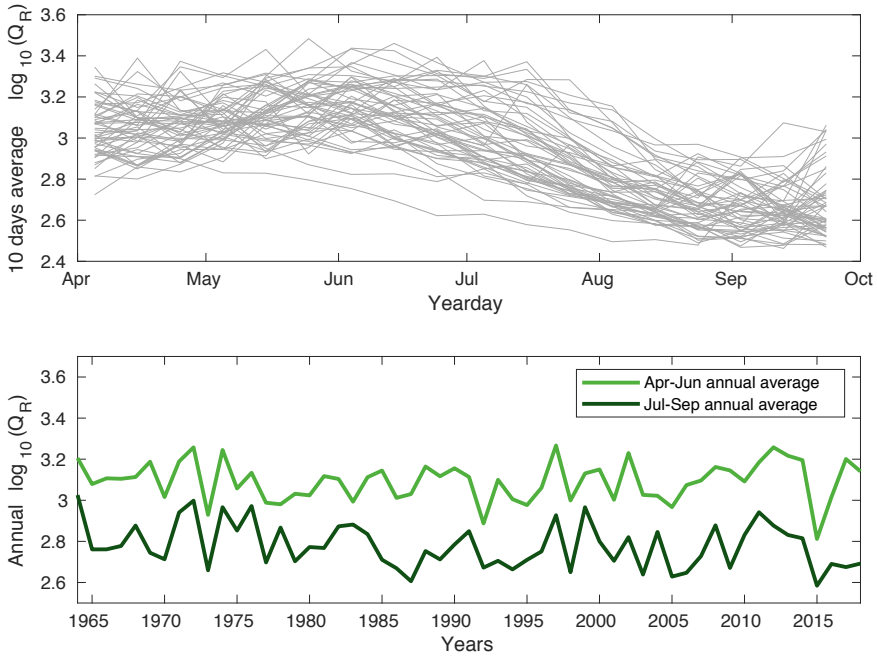

Figure 5: Total riverflow from the eight Puget Sound rivers included in the analysis (see text), shown as *(top)* 10-day averages April–September of individual years, and *(bottom)* annual averages 1964–present.

flows from four rivers that enter Puget Sound up-estuary from the study location (Deschutes, Nisqually, Puyallup and Green), as well as the Cedar, Snohomish, Stillaguamish and Skagit, which supply a much larger freshwater flux that enters Main Basin not far down-estuary (see *Banas et al.* (2014) for mapping of the influence of individual river inputs across seasons in the MoSSea model). Including discharge from all eight of these rivers, instead of only the four up-estuary rivers, slightly increases the Pearson coefficient of the regression analysis below (Sec. 3.1). Most of these observational records run from 1964–present, except for the Deschutes (1991–) and Nisqually (1978–). These rivers with shorter records represent only 1% and 3.8% of total riverflow, respectively.

2.2 Models

Past and new analysis of six models were synthesized in this study (Table 1).

LiveOcean is a coupled physical-biogeochemical forecast model for the Salish Sea and Pacific Northwest outer coast (Fig. 6, built using the Regional Ocean

Table 1: Ocean and atmospheric models used in this study.

Model	Domain	Type	Time period	References
NNRP/WRF	Atmosphere	3D	1950–2010	*Dulière et al.* (2011)
ROMS Cascadia	Coastal ocean	3D	2003–2009	*Stone et al.* (2018)
LiveOcean	Coastal ocean + Salish Sea	3D	2017–2019	
PS-1D	Salish Sea	1D	representative seasonal cycle	this study
SOG	Salish Sea	1D	1968–2010	*Collins et al.* (2009), *Allen and Wolfe* (2013)
CCSM3/WRF/ ROMS	Atmosphere + Coastal ocean + Salish Sea	3D	2040s projection	*Moore et al.* (2015)

Modeling System (ROMS). It has produced continuous 3 d forecasts since 2013, with a switch to much higher resolution (500 m) in the Salish Sea in 2017: in this study we use the archived forecasts from 2017–2018 as a de facto hindcast. LiveOcean is forced by the global ocean model HYCOM on its outer boundary, daily flow estimates for 45 rivers based on USGS gauge data, and high-resolution atmopsheric forcing from a WRF (Weather Research and Forecasting) model run by the UW Mesoscale Analysis and Forecasting Group. *Davis et al.* (2014) describes the model's plankton dynamics in detail, including parameterization and validation using a variety of observations from the outer coast. *Siedlecki et al.* (2015) describes the dissolved-oxygen component.

Two years of hourly physical variables were extracted from LiveOcean along an east–west section line close to PSB003 (Fig. 2). All data were tidally averaged using a Godin filter and subsampled into daily values, and horizontally averaged. Vertical diffusivity κ_v was averaged over the top 20 m, and stratification $\delta\rho$ was defined over the top 20 m as for DOE observations (Fig. 16). This depth range was chosen to isolate processes relevant to phytoplankton growth. Coordinated time series of three driving variables were also defined: wind stress τ at the same section line, rms tidal velocity u_T, and riverflow Q_r from the USGS observations described above.

LiveOcean, and the MoSSea model of Puget Sound which preceeded it (*Sutherland et al.*, 2011), have both been used to quantify the estuarine exchange flow in Puget Sound, although never on the interannual timescale of greatest interest here. Results to date from an unpublished analysis of daily variation in exchange volume flux over 2017 (MacCready et al., in prep.) indicate that the classic theories of estuarine circulation, which would suggest useful scaling relationships between riverflow and the exchange flow, simply do

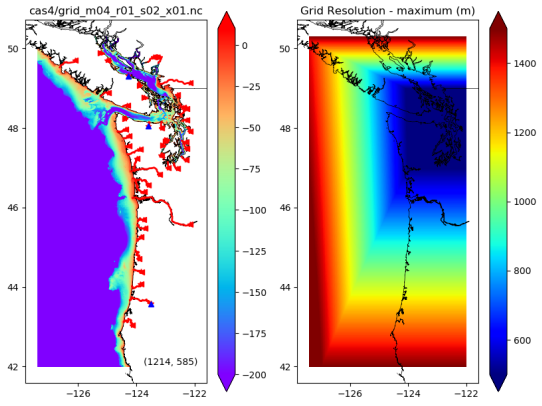

Figure 6: Domain of the LiveOcean model, showing the river inputs included *(left)* atop bathymetry, and horizontal resolution *(right)*.

not apply: tidally averaged volume flux through Admirality Inlet does not increase during periods of increased riverflow, but in fact decreases slightly. This volume flux does show a significant correlation with the along-channel density gradient $d\rho/dx$, its proximate driver (not shown). However, we speculate that $d\rho/dx$ is fundamentally controlled not by total riverflow in Puget Sound (where the largest sources of freshwater are distributed spatially and the largest of all, the Fraser River, in fact enters from the "ocean" end), but rather by gradients in river influence, which are likely modulated by wind as well as by the rivers themselves. Untangling these effects is beyond the scope of this report, and so we treat the exchange flow as an independent environmental driver in its own right, presumably linked strongly to hydrological and atmospheric drivers, but by patterns we cannot presently resolve. LiveOcean results from 2017 are used to set an upper limit on the interannual variability of the seasonally-averaged exchange flow, for comparison with other drivers.

ROMS Cascadia is an antecedent to LiveOcean, a hindcast model that resolves outer-coast physics and biogeochemistry at 1.5 km resolution over the continental shelf and more coarsely offshore, and includes Salish Sea physics—not biogeochemistry—also at 1.5 km resolution, significantly coarser than the 2017– version of LiveOcean used here. *Giddings et al.* (2014) described and validated the model physics for 2004–2007 and *Stone et al.* (2018) subsequently described interannual variation in shelf and slope waters using a 2003–2009 hindcast.

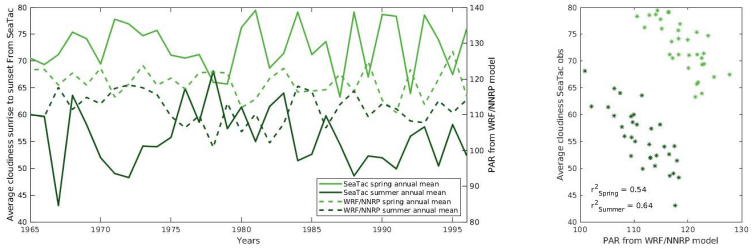

Figure 7: Comparison betwenn NNRP/WRF shortwave radiation and SeaTac observations of cloud cover for summer and spring. Left plot shows both daily time series. Right plot shows the negative correlation between the two time series.

NNRP/WRF is a regional hindcast of weather and climate, 1950–2010. It was constructed by downscaling the global, course-scale atmospheric NCAR/ NCEP Reanalysis (NNRP) with the Weather Research and Forecasting (WRF) model, as described by *Dulière et al.* (2011).

Daily values of wind stress over Main Basin, 1950–2010, were calculated from wind speed at 13 grid points in NNRP/WRF, converted to wind stress following *Large and Pond* (1981) (Fig. 9). To validate these model results, we compared the wind speed time series with data from the SeaTac Airport station (Fig. 8). A step change in the SeaTac observations is visible at the end of the 1990s, likely the result of a change in the anemometer position (*Wan et al.* (2010)). After the step change, NNRP/WRF and SeaTac observations show similar variations.

Daily value of PAR values over Main Basin, 1950–2010, were calculated as 43% of downward shortwave flux at the same 13 grid points in NNRP/WRF. The time series of PAR is well-correlated with sunrise-to-sunset average cloudiness from the SeaTac Airport station, 1965–1996 (Fig. 7).

CCSM3/WRF/ROMS is a regional climate–ocean projection, constructed by downscaling the global CCSM3-A1B model through WRF, and then using this, along with hydrological projections for Puget Sound rivers and the Fraser River, to drive a variant of the ROMS Cascadia model. *Moore et al.* (2015) describe a projection for the 2040s made using this coupled system, in comparison with a "present-day" (1988) reference case, in the context of potential climate impacts on *Alexandrium* HABs. The major forcing changes in this scenario can be summarized as increased air temperatures, a shift toward earlier riverflow, and intensified summer upwelling, all close to the mean of the CMIP3 (IPCC AR4) ensemble, with offshore oceanic boundary conditions held constant. The responses of the marine system to this scenario (*Moore et al.*, 2015) are summarized in Table 2.

SOG is a 1D physical–biogeochemical model for the southern Strait of Georgia designed for hindcasting and prediction of the timing of the spring phytoplank-

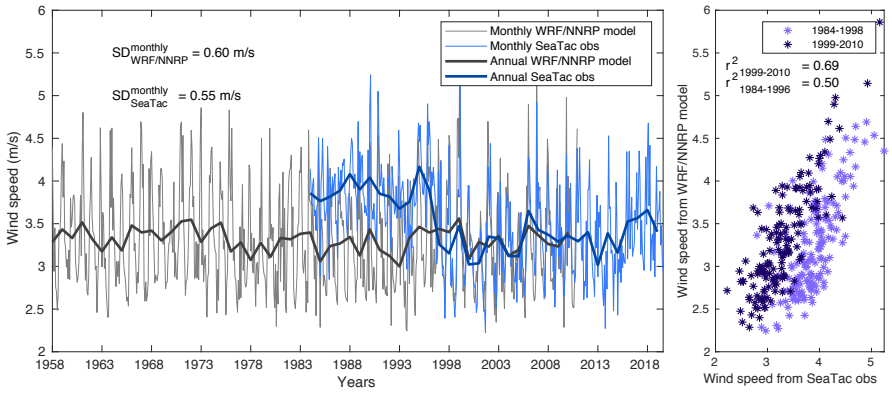

Figure 8: Comparison betwenn NNRP/WRF model output and SeaTac observations of wind stress. Left plot shows both daily time series. Right plot shows SeaTac observation versus WRF/NNRP model output.

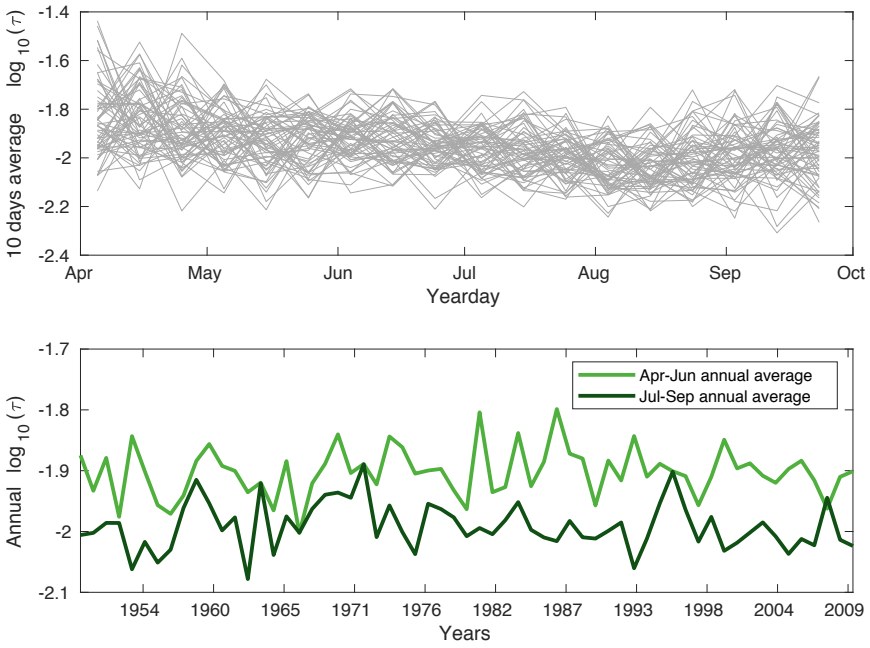

Figure 9: log_{10} wind stress daily output from WRF/NNRP model. *(top)* 10 d averages, 1950–2010, superimposed as a function of yearday. *(bottom)* Spring (Apr–Jun) and summer (Jul–Sep) averages.

Variable	*Change*	*Season*
Wind speed	$\pm$ 0.7 m s^{-1}	spring–summer
Stratification	+ 20%	spring
	$\sim$ 0	summer
Near-surface temperature	+ 2 °C	spring
	+ 3 °C	summer

Table 2: Estimates of future trends in environmental drivers, from a downscaled climate projection (CCSM3/WRF) coupled to ROMS Cascadia as described in *Moore et al.* (2015). Trends are reported as the absolute change between 2040s projections and a baseline circa 1990.

ton bloom, as described in detail by *Collins et al.* (2009) and *Allen and Wolfe* (2013). Here it provides independent estimates of four sensitivities calculated from LiveOcean and PS-1D (albeit in the Strait of Georgia, not Main Basin): the sensitivity of mixing to wind stress, from daily values in 2005 and 2007 hindcasts; the sensitivity of spring bloom date to temperature, as calculated by *Allen and Wolfe* (2013) from a 1968–2010 hindcast; sensitivity of bloom date to light, from Dec–Mar average cloud cover (*Allen and Wolfe*, 2013) and the approximation that as cloud cover varies between 0 and 100%, daily-average PAR varies by $\sim$ 60 W m^{-2}; and the sensitivity of bloom date to mixing, from the sensitivity of bloom date to Dec–Mar average wind stress combined with the mixing–wind relationship already mentioned.

PS-1D is a 1D model designed as a quick-running "sandbox" in which to explore the parameter space of the LiveOcean biogeochemical model (*Davis et al.*, 2014); determine how its parameterization needs to be changed to correctly represent Main Basin as opposed to the offshore waters for which it was originally developed; and perform the numerical experiments which allow us to define scales of sensitivity of each primary-production metric to each environmental driver (Fig. 1). This model has not been previously described in the literature and so we explain it at a medium level of detail below. The full description is expected to appear in *Nguyen* (2020).

2.3 The PS-1D model

2.3.1 Physical setup

The physical "sandbox" of the PS-1D model is designed to reproduce a representative seasonal cycle at one location in central Main Basin, as a base case around which we can perform experiments addressing the sensitivity of phytoplankton dynamics to environmental conditions and to the assumed biological parameters. These analyses have more the flavor of laboratory or mesocosm experiments than historical analysis—doubling the turbulent mixing, halving the incoming light, etc.—and do not attempt to resolve event-scale fluctuations, for which a 1D model would likely be fundamentally inappropriate.

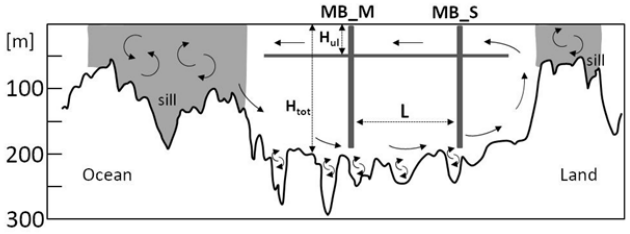

Figure 10: Schematic of physical processes in Main Basin. The study site lies midway between MB_M and MB_S, which define the span used to estimate along-channel gradients.

In this 1D model, a water column of $\sim$ 200 meter depth was divided into thirty layers, with thinner layers near the surface and thicker layers at the bottom. Within this grid, the model consists of a set of coupled ordinary differential equations, each one a budget for one biogeochemical tracer (see Sec. 2.3.2).

Advection The upward velocity w_{adv} representing the estuarine exchange flow depends, because of mass conservation, on the along-channel gradient in the lower-layer incoming volume flux (Fig. 10). The mid-water-column maximum in w_{adv} (Fig. 11) was estimated from the MoSSea model (*Sutherland et al.*, 2011) as $\Delta Q\ L^{-1}\ B^{-1}$, where $\Delta Q = 3500$ m^3 s^{-1} is the difference in lower-layer volume fluxes between MB_M and MB_S, $L = 26$ km is the distance between the two sections, and $B = 5$ km is the channel width. In tuning and sensitivity experiments below, the shape of the vertical profile of w_{adv} was kept constant and multiplied by a factor representing increases and decreases in the exchange flow.

Observations of chlorophyll, nitrate and ammonium of PRISM stations along Puget Sound (black solid points in Fig. 2) in June and December showed negligible gradients in Main Basin (around 10^{-3} at PSB003: not shown). The small gradients are consistent with the conclusion of *Winter et al.* (1975) that horizontal advection is not an important term in the budgets of these tracers in Main Basin.

Vertical mixing The vertical diffusivity for tracers κ_v was likewise taken from the 2006 hindcast of the MoSSea model. A climatological vertical profile was constructed by taking the cross-sectional average diffusivity as a function of depth (Fig. 12, black dots) and then averaging in time (blue line). As analysed further below using LiveOcean output, monthly or seasonal variation in mixing appears to be secondary to shorter-timescale variation, and so we have held mixing constant in our representative seasonal cycle. As for vertical advection, experiments in which the intensity of mixing is varied multiply this mean profile by a constant.

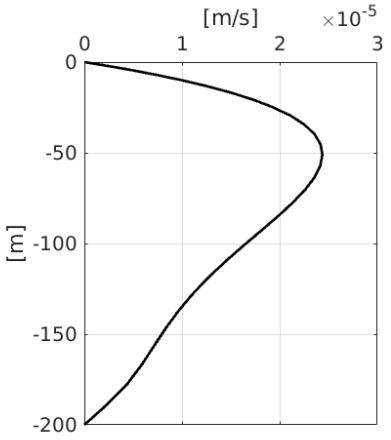

Figure 11: Vertical velocity profile in the base case of PS-1D.

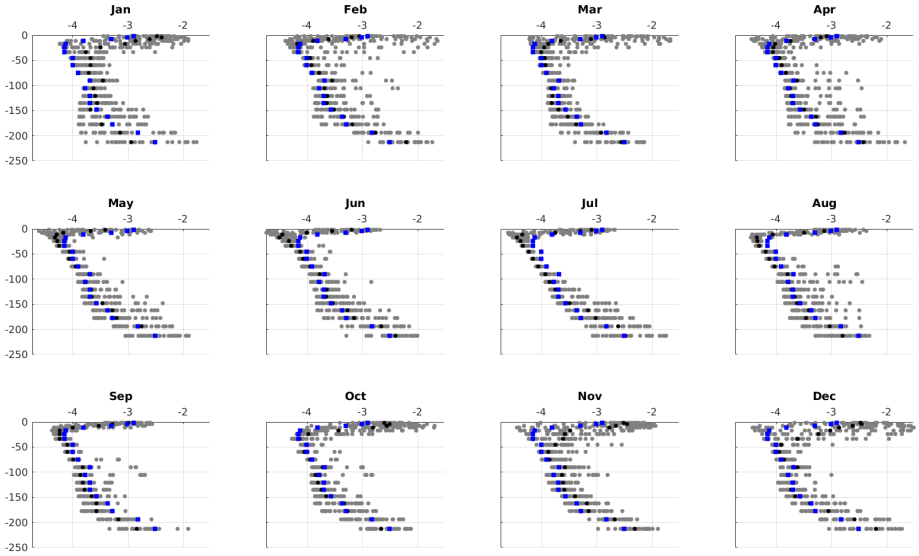

Figure 12: Vertical profiles of the vertical diffusivity for tracers, cross-sectionally averaged in one year of 3D model output (MoSSea, 2006: *Sutherland et al.* (2011)). Black dots show daily values, grouped by month, and the blue line (repeated across panels) is the climatological profile used in the PS-1D base case.

Light Surface light in PS-1D is taken directly from the regional weather model used to drive MoSSea. Photosynthetically active radiation (PAR) is assumed to be 43% of downward shortwave radiation. PAR at a given depth, $E(z)$, is modelled using three light-attenuation coefficients as

$$E(z) = E_0 \ \exp\left[-(att_{bg}\ z + att_{fw}\int_z^0 (32 - S(z'))dz' + att_P \int_z^0 P(z')dz'\right] \quad (1)$$

where E_0 is PAR at the surface ($z = 0$). The coefficient att_{bg} is the per-meter attenuation by pure seawater; att_{fw} represents attenuation by particles and dissolved organic matter associated with freshwater (mathematically speaking, attenuation that is correlated with salinity deficits); and att_P represents light attenuation by the modelled phytoplankton themselves, i.e., self-shading.

These are crucial model parameters, and among the most likely to vary between estuarine and coastal environments. Prior to running the model, historical Puget Sound observations were used to estimate these coefficients and determine if they substantially different from the values found by *Davis et al.* (2014) for the Washington–Oregon shelf. Euphotic-zone depths from three years of monthly transmissometer profiles (*Newton and Van Voorhis*, 2002) agreed well with Secchi Disk depths, which makes euphotic-zone depths a good source to estimate light fields. A linear regression of light attenuation (back-calculated from euphotic depth) and chlorophyll, omitting winter samples, showed high correlation ($R^2 = 0.7$) in the *Newton and Van Voorhis* (2002) dataset. However, light attenuation is commonly expected to depend on constituents of freshwater as well, and so we used the full record of 19 years (1999 - 2017) DOE sampling at PSB003, which provides coordinated observations of beam attenuation, chlorophyll, salinity, and turbidity. An empirical relationship from *Shannon* (1975) was used to convert beam attenuation to light attenuation. Turbidity and salinity are highly correlated in the PSB003 dataset, and a linear regression for light attenuation as a function of chlorophyll and salinity (as in Eq. (1)) showed high correlation ($R^2 = 0.64$) and tight bounds on coefficients.

The estimate of light attenuation by chlorophyll from this linear model (0.023) was consistent with that derived from the *Newton and Van Voorhis* (2002) three-year dataset described previously (0.026). However, a regression to the PSB003 data omitting salinity explained almost as much variance as the model with salinity. This suggests that salinity or freshwater fraction is not an effective proxy for light attenuation by river-derived material in Puget Sound, possibly because freshwater in Puget Sound originates in such a diversity of watersheds (*Cuo et al.*, 2009; *Banas et al.*, 2014). Thus in PS-1D, att_{fw} is set to 0, not to imply that river inputs do not cause light attenuation, but to indicate that we lack a useful predictor of this effect. Instead, the mean effect of watershed-derived turbidity and dissolved organic matter is captured in the background light attenuation att_{bg}, which is far higher than attenuation by undiluted seawater in the *Davis et al.* (2014) model currently used in LiveOcean (Table 3).

2.3.2 Phytoplankton dynamics

The biogeochemical model in PS-1D is a six-compartment nitrogen budget, nitrate (NO_3), ammonium (NH_4), phytoplankton biomass (P), microzooplankton biomass (Z), and small and large detritus (SD, LD). All six stocks are measured in mmol nitrogen m^{-3} = μM N; we assume a chlorophyll:nitrogen ratio of 2.5 (mg chl) $(\text{mmol N})^{-1}$ to compare the model with observations. Apart from dividing the dissolved inorganic nutrient pool into NO_3 and NH_4 fractions (to match available observations), the model structure and functional forms closely follow *Davis et al.* (2014), who provide a thorough description, rationale, and validation against nutrient, biomass, and growth- and grazing-rate data from the outer coast. Only the phytoplankton component is described below.

Phytoplankton growth rate μ at a given depth and time, as function of PAR E and nutrients, is given by

$$\mu(E, NO_3, NH_4) = \mu_0 \left(\frac{N_{tot}}{k_{min} + 2\sqrt{k_{min} N_{tot}} + N_{tot}} \right) \left(\frac{\alpha E}{\sqrt{\alpha^2 E^2 + \mu_0^2}} \right) \quad (2)$$

where the effective total nutrient concentration N_{tot} is given by

$$N_{tot} = NO_3 + \varphi_{\mathrm{NH4}} NH_4 \quad (3)$$

The uptake preference $\varphi_{\mathrm{NH4}} = 2$ to take into account that NH_4 is taken up faster than NO_3. The first bracketed quantity is a nutrient-limitation factor, similar to a Michaelis-Menten (Holling type II) saturating response, but incorporating the "optimal uptake" model of *Smith et al.* (2009). The second bracketed quantity is a light-limitation factor, written in terms of the initial slope of the photosynthesis-irradiance curve α. E depends on depth and phytoplankton concentration P according to Eq. (1).

As in the original *Davis et al.* (2014) model, there is no explicit dependence on temperature; μ_0 and other vital rates in the model are defined at typical ambient temperatures, and we assume the temperature-driven change in these rates during one simulation is small compared with other modes of variation and uncertainty (e.g. changes in species composition, or error in the nutrient or light-limitation formulations). However, in the sensitivity analysis below, we quantify the likely effect of temperature by adjusting μ_0, along with maximum grazing rate and remineralization rate, by a factor ${Q_{10}}^{\Delta T/10^{\circ}\mathrm{C}}$ for a mean temperature shift of ΔT. We assume $Q_{10} = 2$, a common rule of thumb for temperature response in phytoplankton (*Eppley*, 1972; *Bissinger et al.*, 2008).

Each model simulation is two years, with the annual cycle repeated exactly, and the first year discarded as spinup. The model is initialised based on the time-average and depth-average of December observations, when the water column is close to homogeneous: initial NO_3 concentration is 27.85 μM N, and the same value is imposed as a bottom boundary condition (at 200 m depth) over the course of the simulation, as a simple means of representing the continual resupply of nutrients via the estuarine circulation.

2.3.3 Parameter optimisation

Apart from the light attenuation parameters, which were defined from historical data as described above, and parameters that are essentially structural choices or assumed to be universal, there are 11 parameters in the biogeochemical model that might plausibly differ between the Puget Sound and outer-coast ecosystems, and thus require a systematic investigation before settling on an adaptation of the *Davis et al.* (2014) model for use in PS-1D.

The 11 unknown parameters were tuned using "particle swarm optimisation" (PSO, *Poli et al.* (2007)). In PSO a number of imagined entities—the "particles"—are placed in a search space that consists of a summary measure of goodness-of-fit, the "cost," as a function of the parameters being tuned. Each particle then determines its movement through the search space by combining aspects of the history of its own search (its current position and the best fit/lowest cost previously found) with the best fit found across the other members of the swarm, as well as random perturbations. Eventually the swarm as a whole, like a flock of birds collectively foraging for food, is likely to converge on the global optimum of the fitness function.

The cost function was defined using the Willmot skill score

$$WSS_{MAE} = 1 - \frac{\frac{1}{N}\sum_{i=1}^{i=N}|m_i - o_i|}{\frac{1}{N}\sum_{i=1}^{i=N}\left(|m_i - \bar{o}| + |o_i - \bar{o}|\right)} \tag{4}$$

where m_i and o_i are N matched pairs of model estimates and observations of chlorophyll (Chla), nitrate (NO_3) and ammonium (NH_4).

The PSO was run for 300 iterations until each of the 11 parameters converged, after which we ran a set of 11 experiments varying one parameter at a time, in order to determine whether model behaviour was sensitive to the difference between the PSO-derived value and the original *Davis et al.* (2014) value (Fig. 13). Results allowed us to rank the PSO-derived parameters from greatest effect on model behaviour (initial growth-light slope (α), phytoplankton mortality (m_P) to least (sinking rate of detritus, aggregation rate of phytoplankton). This indicates that there are indeed some, but fewer than 11, parameters in the LiveOcean biogeochemical model that need to be changed in order to correctly describe Main Basin. To make a final, practical decision regarding which parameters to change, the PSO-derived parameter set was replaced by the original values one at a time, and the series of changes in WSS assessed: at the end, initial growth-light slope α, phytoplankton mortality m_P, zooplankton grazing half-saturation K_0, maximum phytoplankton growth rate μ_0, nitrification rate r_{nitr}, and remineralization rate r_{remin} were changed (Table 3).

Model outputs using the final tuned parameters showed good agreement with the observed seasonal cycle of euphotic-zone-integrated NO_3 (Fig. 14). The model captures phytoplankton bloom timing accurately, as well as mean spring–summer concentrations, but does not show transient peaks as high as some seen intermittently in spring and summer data. The model's winter and summer ammonium concentrations are consistent with observations.

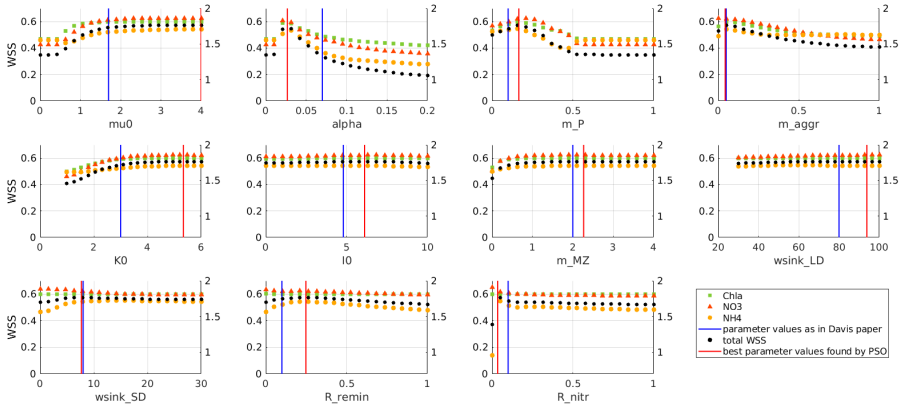

Figure 13: Results from varying one parameter at a time around the set of optimised parameters. The original *Davis et al.* (2014) parameter values (blue lines) and PSO-derived values (red lines) are indicated. Left y–axis shows model behaviour of chlorophyll (Chla, green squares), nitrate (NO_3, red triangles), and ammonium (NH_4, orange circles), and right y–axis is for model as a whole (black circles). X–axes are ranges of parameters in which they are varied.

Parameter	**Description**	**Unit**	**Davis et al.**	**PS-1D**
att_{bg}	Light attenuation by water column	m^{-1}	0.05	**0.15**
att_{fw}	Light attenuation by fresh water	m^{-1}	-0.0065	**0**
att_P	Light attenuation by phytoplankton	m^{-1} μM N^{-1}	0.03	**0.026**
μ_0	Maximum phytoplankton growth rate	d^{-1}	1.7	**4**
k_{min}	Minimum half-saturation for NO_3	μM N	0.1	0.1
α	Initial growth-light slope	(W m^{-2})$^{-1}$ d^{-1}	0.07	**0.027**
φ_{NH_4}	Preference for NH_4		2	2
m_P	Phytoplankton mortality	d^{-1}	0.1	**0.163**
m_{agg}	Phytoplankton loss via aggregation	(μM N)$^{-1}$ d^{-1}	0.05	0.05
I_0	Zooplankton maximum ingestion rate		4.8	4.8
K_0	Zooplankton grazing half-saturation	μM N	3	**5.3**
ϵ	Microzooplankton growth efficiency		0.3	0.3
m_{MZ}	Microzooplankton mortality	d^{-1}	2	2
f_{ex}	Fraction of grazing excreted to NH_4		0.5	0.5
r_{remin}	Detrital remineralisation rate	d^{-1}	0.1	**0.25**
$w_{s_{SD}}$	small detritus sinking rate	m d^{-1}	8	8
$w_{s_{LD}}$	large detritus sinking rate	m d^{-1}	80	80
r_{nitr}	Nitrification rate		0.1	**0.035**

Table 3: Final PS-1D tuned parameters for Main Basin, compared with *Davis et al.* (2014) values for the outer coast. μMN = mmol nitrogen m^{-3}.

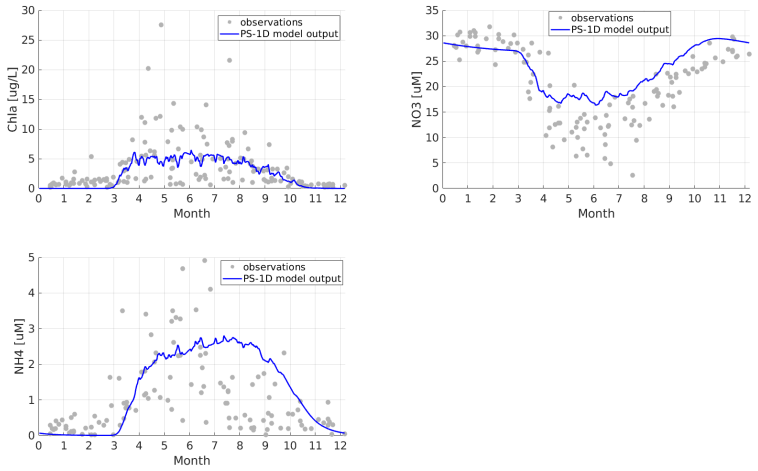

Figure 14: Final PS-1D model outputs (blue line) against observations (gray solid points) of chlorophyll (Chla), nitrate (NO_3), and ammonium (NH_4). Chla, NO_3, and NH_4 were calculated as average integratal over euphotic depth

2.4 Integration of models and observations

The PS-1D model just described is our principal means of quantifying the sensitivity of various measures of phytoplankton production to environmental factors, including turbulent mixing, while the SOG model provides a point of comparison for several of these estimates. We use five phytoplankton metrics (*i*–*iv* in Sec. 1, with *iii*) subdivided):

1. Total annual primary production PP_{tot}, converted to units of g C m^{-2} yr^{-1} assuming a C:N ratio of 106:16 mol:mol;

2. Date of the spring bloom t_{bloom}, defined as the day of year when cumulative, vertically-integrated phytoplankton biomass reached 15% of its annual total;

3. Phytoplankton concentration during the seasonal period and depth layer associated with steelhead outmigration ($P_{outmigr}^{steelhead}$), mid April–first week of June (yeardays 109–159), and 0–2 m depth;

4. Phytoplankton concentration during chinook outmigration in summer $P_{outmigr}^{chinook}$, first week of June–mid September (yeardays 159–258), 0–15 m depth;

5. Incidence of strong nutrient stress in summer Δt_{nut}, defined as the count of days on which surface nutrient concentration is less than 3 mmol m^{-3}.

The LiveOcean model, along with historical observations, provides the means of determining the relationships between turbulent mixing and riverflow, wind

stress, stratification. Mixing intensity, riverflow, stratification, and wind stress magnitude were all log-transformed, so that power-law relationships among them can be described by constant sensitivities: if a driver D and response R are related by $R = aD^b$, then a and b can be estimated by a linear regression between $\log D$ and $\log R$, and the sensitivity of R to D is given by

$$\frac{\partial(\log R)}{\partial(\log D)} \equiv b \tag{5}$$

As described above, a combination of observations and model hindcasts/projections allows us to quantify variability in the atmospheric, oceanic, and watershed drivers themselves. Relating these scales of variability in drivers to the associated variability in phytoplankton metrics is a matter of multiplication and the chain rule: for example, the variability in spring bloom date t_{bloom} associated with interannual variability in spring wind stress τ, via the effect of wind stress on turbulent mixing ($\mathbf{E} \rightarrow \mathbf{K} \rightarrow \mathbf{L}$, Fig. 1), is given by

$$\Delta t_{bloom} = \Delta(\log_{10} \tau) \cdot \frac{\partial(\log_{10} \kappa_v)}{\partial(\log_{10} \tau)} \cdot \frac{\partial t_{bloom}}{\partial(\log_{10} \kappa_v)} \tag{6}$$

In general, each arrow in Fig. 1 represents one sensitivity, or partial derivative like the two that appear in 6, although the distinction in Fig. 1 between mechanisms that affect light limitation and mechanisms that affect nutrient limitation is a matter of interpretation rather than an explicit calculation. This analysis is a scaling exercise, and we endeavour not to overinterpret differences that are smaller than a factor of three.

The primary timescale of analysis is interannual variation in seasonal averages, i.e. the variance of Apr–Jun (spring) or Jul–Sep (summer) averages across a number of years. (Scales of variation denoted by Δ are defined throughout as 2 standard deviations.) In some cases, we have no means of calculating interannual variation in this way: for example, variation in the exchange flow (and hence vertical advection, under our assumptions) has been calculated across one annual cycle in LiveOcean (MacCready et al., in prep) but never across a useful ensemble of years. In these cases, we interpret the known event-scale (10 d) variation as a high upper bound on the unknown interannual variation. In other cases, it is not clear whether seasonal averages are indeed the timescale on which the environment drives variation in phytoplankton dynamics. For example, across three years of data from a high-time-resolution profiling buoy in Carr Inlet in South Puget Sound (ORCA, 2011–2013, *https://nwem.apl.washington.edu/about_proj_ORCA.shtml*), it is possible to identify three events in which a transient peak in stratification is followed by a transient phytoplankton bloom (arrows, Fig. 15); whereas correlations between stratification and chlorophyll on the monthly scale and longer are weak to nonexistent. Thus we calculated and report event-scale (10 d) variation for select quantities as an aid to interpretation and source of follow-on hypotheses.

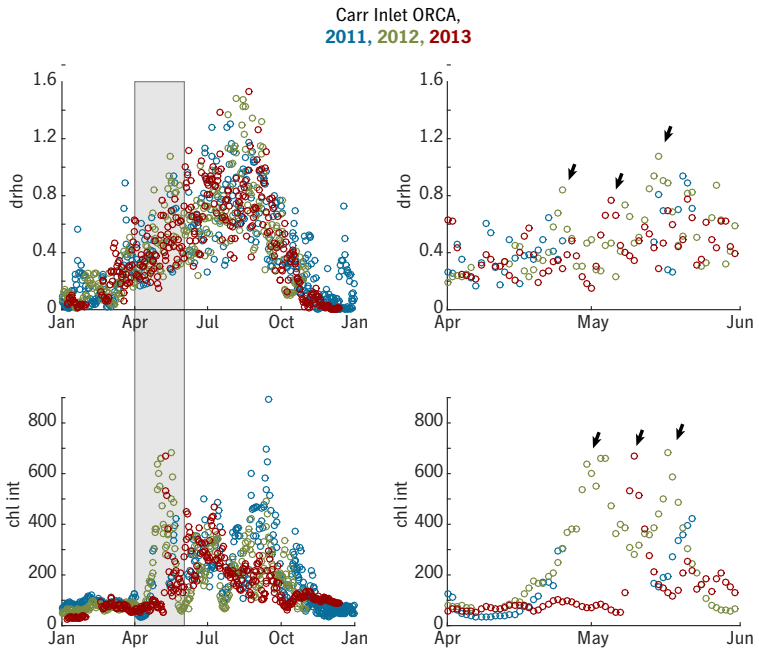

Figure 15: Bottom–surface density difference ("drho," , in $sigma_t$ units) and chlorophyll (vertically integrated, mg m^2) at the Carr Inlet ORCA buoy, for 2011 (blue), 2012 (green), and 2013 (red). Each point represents one day. The shaded time period in the left panels is expanded in the right panels. Three event-scale phytoplankton blooms associated with event-scale peaks in stratification are marked with arrows.

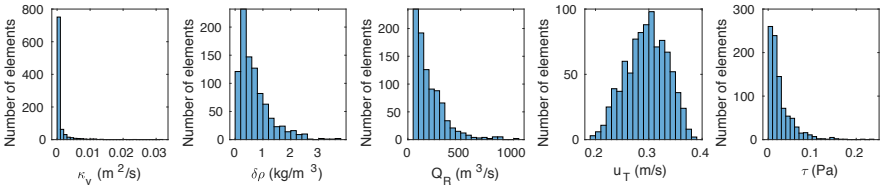

Figure 16: Histograms of stratification, mixing and environmental forcing at a section across central Main Basin, from the LiveOcean model, 2017–2018.

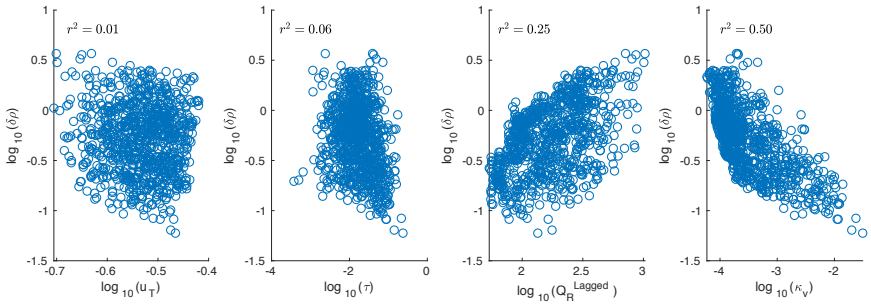

Figure 17: Scatter plots of stratification $\log_{10}\delta\rho$ versus drivers.

3 Results

3.1 Dynamics of stratification and mixing

In the time series derived from LiveOcean, stratification $\delta\rho$ is significantly correlated with and mixing κ_v and riverflow Q_r with maximum lagged correlation occuring for 8 days of lag (Fig. 17). It is not significantly correlated with wind stress τ and tidal velocity u_T. These results are consistent with a classical view of estuarine circulation in which stratification primarily reflects the competition between the homogenizing effect of mixing and the stratifying effect of river discharge. Near-surface mixing κ_v is significantly correlated with wind stress τ and stratification $\delta\rho$, but not tidal velocity u_T or river discharge Q_r (Fig. 18). Variation in near-bottom mixing is, in contrast, primarily explained by the tides (not shown).

These results suggest a two-step approach in which we first predict mixing as a function of wind stress and stratification via a multiple regression on LiveOcean time series, yielding a pair of useful sensitivities (Table 4); and second find the sensitivity of stratification to riverflow directly from DOE observations (Fig. 19).

The sensitivity of stratification to temperature is derived directly from the

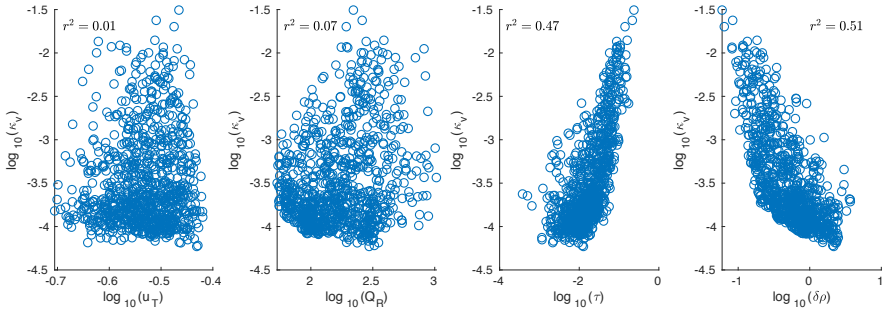

Figure 18: Scatter plots of mixing $\log_{10} \kappa_v$ versus drivers.

linearised equation of state of seawater (Table 4). The simplifying assumption that surface warming has no effect below 20 m makes this value—which indicates a very small effect in any case—an upper bound.

3.2 Environmental variation and phytoplankton dynamics

Results from sensitivity experiments in PS-1D are summarised in Table 5. Each row describes a family of model runs in which one driving variable at a time was varied around its base-case value. Sensitivities are not normalised and are expressed in disparate units, and thus are difficult to evaluate in themselves; they constitute an intermediate step in the overall scaling analysis. Independent estimates of the sensitivity of spring bloom date to mixing, temperature, and light (in the southern Strait of Georgia, not Main Basin) were also calculated from the SOG model (Table 5), as described in Sec. 2.2.

Means and scales of variation for all other quantities required for the final scaling analysis are given in Table 6. Scales of variation in turbulent mixing ($\log_{10} \kappa_v$) are derived from the sensitivities reported in Table 4. Other quantities are derived directly from observational and model time series as described in Sec. 2.

As expected, variation in riverflow, wind stress, and PAR is markedly larger on the 10 d scale than in seasonal averages. This result is true for both spring (Apr–Jun) and summer (Jul–Sep) records. On the event scale, wind and riverflow/stratification drive strong variability in turbulent mixing of similar magnitude (approximately $\pm$ 0.2 in $\log_{10}$ units, or 60%), while on the interannual scale, wind stress variations largely average out and drive much less variance in mixing ($\pm$ 0.05 vs. 0.12–0.14 in $\log_{10}$ units, or 10% vs. 32–38% variation).

The final quantification of the various mechanistic pathways leading to phytoplankton dynamics (Fig. 1) is summarised in Table 7, which combines estimates of variability in drivers (Table 6) with estimates of sensitivities (Tables 4 and 5), as in Eq. (6). Results are given for the interannual timescale, using

Near-surface mixing as a function of stratification and wind stress			
Regression equation	$\log_{10}\kappa_v = a + b \cdot \log_{10}\rho_z + c \cdot \log_{10}\tau$		
Intercept	a	-2.56 ± 0.57	LiveOcean, 2017–2018
Sensitivity of mixing to stratification	$b \equiv \frac{\partial(\log_{10}\kappa_v)}{\partial(\log_{10}\delta\rho)}$	-0.89 ± 0.37	LiveOcean, 2017–2018
Sensitivity of mixing to wind stress	$c \equiv \frac{\partial(\log_{10}\kappa_v)}{\partial(\log_{10}\tau)}$	0.67 ± 0.29	LiveOcean, 2017–2018
		0.83	SOG
Other sensitivities			
Sensitivity of stratification to riverflow	$\frac{\partial(\delta\rho)}{\partial Q_r}$	1.87 1.14	DOE obs., spring summer
Sensitivity of stratification to surface temperature	$\frac{\partial(\delta\rho)}{\partial T_{20}}$	0.18	Equation of state at 30 psu, 12°C; assumes no change below 20 m

Table 4: Relationships among vertical diffusivity, stratification, riverflow, wind stress, and temperature.

spring values from Table 6 for t_{bloom} and $P^{steelhead}_{outmigr}$, summer values for $P^{chinook}_{outmigr}$ and δt_{nut}, and whichever is larger in each case for PP_{tot}. Estimates are also given for long-term change over 50 y, under the single climate projection used in CCSM3/WRF/ROMS (Table 2). Estimates of spring-bloom-date variation based on event-scale variability in the drivers, as opposed to seasonal averages, are also shown; the analogous calculations for the other phytoplankton metrics, which describe seasonal patterns rather than events, would not be interpretable. However, the expected variability driven by the exchange flow (via w_{adv}) and via changes in light attenuation are expressed as "much less than the variability one would calculate based on event-scale changes in w_{adv} and att_{bg}," since we lack a basis for quantifying the interannual variation in seasonal averages of these drivers.

Results are given in the same units as the base-case values of the five metrics, which are also shown in Table 7 for comparison. For each metric, the scale-setting, largest effects are marked with a $**$, and other effects within half an order of magnitude, or a factor of 3, are marked with a $*$. These categories together are considered "major effects" and the others are considered "minor."

Either variation in surface PAR or the effect of riverflow on turbulent mixing (via stratification) is the scale-setting driver for each of the five metrics, and the effect of light attenuation is consistently in the class of potential major effects. Interannual variation in N_{deep} does not have a major effect on any of the phytoplankton metrics. Other drivers (wind stress, the exchange flow,

Sensitivity of → to ↓		Annual primary production	Date of spring bloom	Phyto. conc. during steelhead outmigration (spring, 0–2 m)	Phyto. conc. during chinook outmigration (summer, 0–15 m)	Duration of strong nutrient stress (summer)
		PP_{tot} (gC m^{-2} yr^{-1})	t_{bloom} (yearday)	$P^{steelhead}_{outmigr}$ (mg C m^{-3})	$P^{chinook}_{outmigr}$ (mg C m^{-3})	δt_{nut} (d)
$\log_{10}\kappa_v$	($\log_{10}$ m^2 s^{-1})	−32	20 *70* (SOG)	−9.4	3.5	−72
w_{adv}	(m d^{-1})	−78	7.6	0.52	0.32	−23
N_{deep}	(μM N)	8.9	0	0.23	0.31	−2
T_{20}	(°C)	15	−1.5 *4.7* (SOG)	0.21	−0.03	3.5
E_0	(W m^{-2})	20	−0.88 *−2* (SOG)	0.38	0.35	1
att_{bg}	(m^{-1})	−5700	150	−48	−78	−600

Table 5: Response of phytoplankton metrics (columns) to variability in physical drivers (rows). All values are derived from senstivity experiments in PS-1D except for three values estimated from SOG for comparsion.

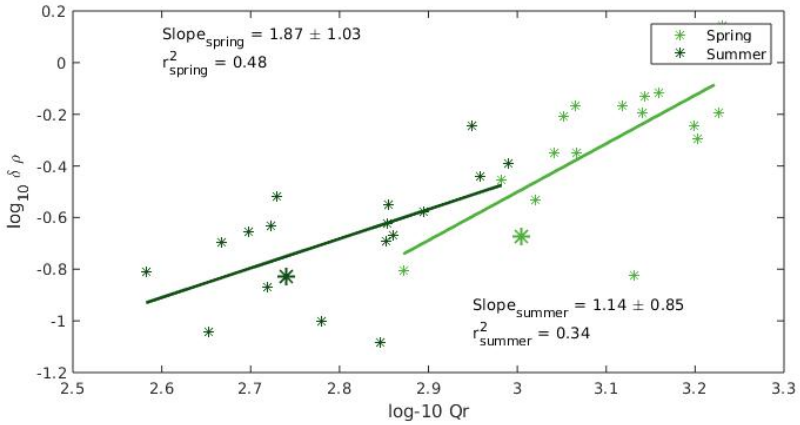

Figure 19: Relationship between $\log_{10}$ stratification (5–20 m density minus 0–5 m density) and $\log_{10}$ riverflow (summed for the eight rivers discussed in Sec. 2.1) in historical observations. Separate regressions are shown for spring (light green) and summer (dark green), although the slopes of these regressions are not significantly different (p ¿ 0.05). A larger marker is used to highlight the drought year 2001 discussed by *Newton et al.* (2003).

near-surface temperature) are found to have potentially major effects on some metrics but not others.

4 Discussion

The results in Table 7 suggest useful simplifications to the tangle of mechanistic pathways in our initial conceptual model. Refined conceptual models for each phytoplankton metric are shown in Fig. 20.

4.1 Primary production

Annual primary production, perhaps by integrating over so many transient aspects of the plankton dynamics, shows the clearest results, the strongest separation between major and minor effects. Variation in light limitation outweighs variation in nutrient limitation, in the sese that an increase in vertical mixing (which decreaes light exposure but increases nutrient supply) has an overall negative effect on PP_{tot} seasonally-averaged incoming PAR appears to be sufficient to drive $\sim$ 15% variation in annual primary production (Table 7). Sample-to-sample variation in background light attenuation—i.e. all effects of water-mass variation and freshwater influence, excluding self-shading by phytoplankton—is on the same scale (att_{bg} = 0.15 $\pm$ 0.03 m^{-1}: Table 3) and varying att_{bg} on this scale in the PS-1D model also leads to $\sim$ 15% changes in PP_{tot}, but we expect that much of this variability in att_{bg} averages out on seasonal timescales.

Quantity	*Units*	*Symbol*	*Mean*	*Log mean*	*Interannual variation* (2 s.d.)		*Event-scale variation* (2 s.d.)		*Comments*	*Source*
			$(\overline{x})$	$(\overline{\log_{10} x})$	Δx	$\Delta(\log_{10} x)$	Δx	$\Delta(\log_{10} x)$		
Riverflow	$m^3\ s^{-1}$	Q_r	1300	3.1		0.19		0.28	spring	USGS obs.,
			680	2.8		0.22		0.38	summer	1964–2018
Wind stress	Pa	τ	0.015	-1.9		0.082		0.24	spring	NNRP/WRF,
			0.012	-2		0.078		0.22	summer	1950–2010
Stratification	$kg\ m^{-3}$	$\delta\rho$	1.25	0.04				0.44	spring	LiveOcean,
			0.57	-0.3				0.44	summer	2017–2018
Temperature	°C	T_{20}	10.2		1.2				0–20 m, spring	DOE obs.
			12.9		0.8				summer	
Mixing	$m^2\ s^{-1}$	κ_v	2.5×10^{-4}	-3.8		0.05		0.16	spring, via τ	see Table 4
						0.12		0.17	spring, via $\delta\rho$, Q_r	
			2.0×10^{-4}	-3.8		0.05		0.15	summer, via τ	
						0.14		0.24	summer, via $\delta\rho$, Q_r	
Surface PAR	$W\ m^{-2}$	E_0	119		8.6		34		spring	NNRP/WRF,
			112		8.6		43		summer	1950–2010
Ocean sourcewater density	$kg\ m^{-3}$	$\Delta\rho_{oc}$			0.02					continental slope, ROMS Cascadia,
Ocean sourcewater nutrients					1.4					2002–2009
Main Basin deep nutrients	$mmol\ m^{-3}$	N_{deep}	27.6		2.8					DOE obs., December
Exchange flow volume transport	$m^3\ s^{-1}$	Q_{ex}	3500				1500			LiveOcean, 2017
Vertical advection	$m\ day^{-1}$	w_{adv}	2.34				0.99		derived from Q_{ex}	
Background light attenuation	m^{-1}	att_{bg}	0.15				0.03		confidence limits on regression	

Table 6: Estimates of environmental variability used in the scaling analysis.

	Annual primary production		Date of spring bloom			Phyto conc. during steelhead outmigration (spring, 0–2 m)		Phyto conc. during chinook outmigration (summer, 0–15 m)		Duration of strong nutrient stress	
	PP_{tot}		t_{bloom}			$P^{steelhead}_{outmigr}$		$P^{chinook}_{outmigr}$		δt_{nut}	
Base-case value	1140 gC m^{-2} yr^{-1}		127 yearday			27 mg C m^{-3}		36 mg C m^{-3}		8 d	
Scale of variability in $\rightarrow$ *via* $\downarrow$	*50 y*	*Interann.*	*50 y*	*Interann.*	*Event*	*50 y*	*Interann.*	*50 y*	*Interann.*	*50 y*	*Interann.*
Wind stress τ (via mixing)	5	2	0	1.1	3.3	0	0.52	0.57	0.19	$\pm$ 11	4
Riverflow Q_r (via stratification and mixing)	5.1	10	-3.7	7.5**	13*	1.8	3.5**	0	0.79	0	16**
Exchange flow Q_{ex} (via vertical advection)		$\ll$ 73		$\ll$ 7.5*	7.5		$\ll$ 0.51		$\ll$ 0.32		$\ll$ 23*
Deep nutrient concentration N_{deep}		25		0			0.64		0.87		2.8
Near-surface temperature T_{20}	30	18	-3	1.8		0.42	0.25	-0.09	0.024	11	2.8
Surface PAR E_0		170**		7.6**	38**		3.3**		3**		8.6*
Background light attenuation att_{bg}		$\ll$ 170*		$\ll$ 4.5*	4.5		$\ll$ 1.4*		$\ll$ 2.3*		$\ll$ 18*

Table 7: Scales of variation in five metrics of phytoplankton production (PP_{tot}, etc.) associated with seven climate-linked drivers (τ, etc.). *Interann.* and *Event* indicate interannual variation in seasonal averages, and variation among 10 d averages within one season, respectively, and are given as an absolute value corresponding to 2 s.d. of variation in the driver. *50 y* indicates total change between $\sim$ 1990 and the 2040s in the CCSM3/WRF/ROMS regional climate projection, a signed quantity. ** indicates the largest or scale-setting process for each metric, and * denotes other mechanisms whose effects are potentially of the same order of magnitude (i.e. within a factor of 3).

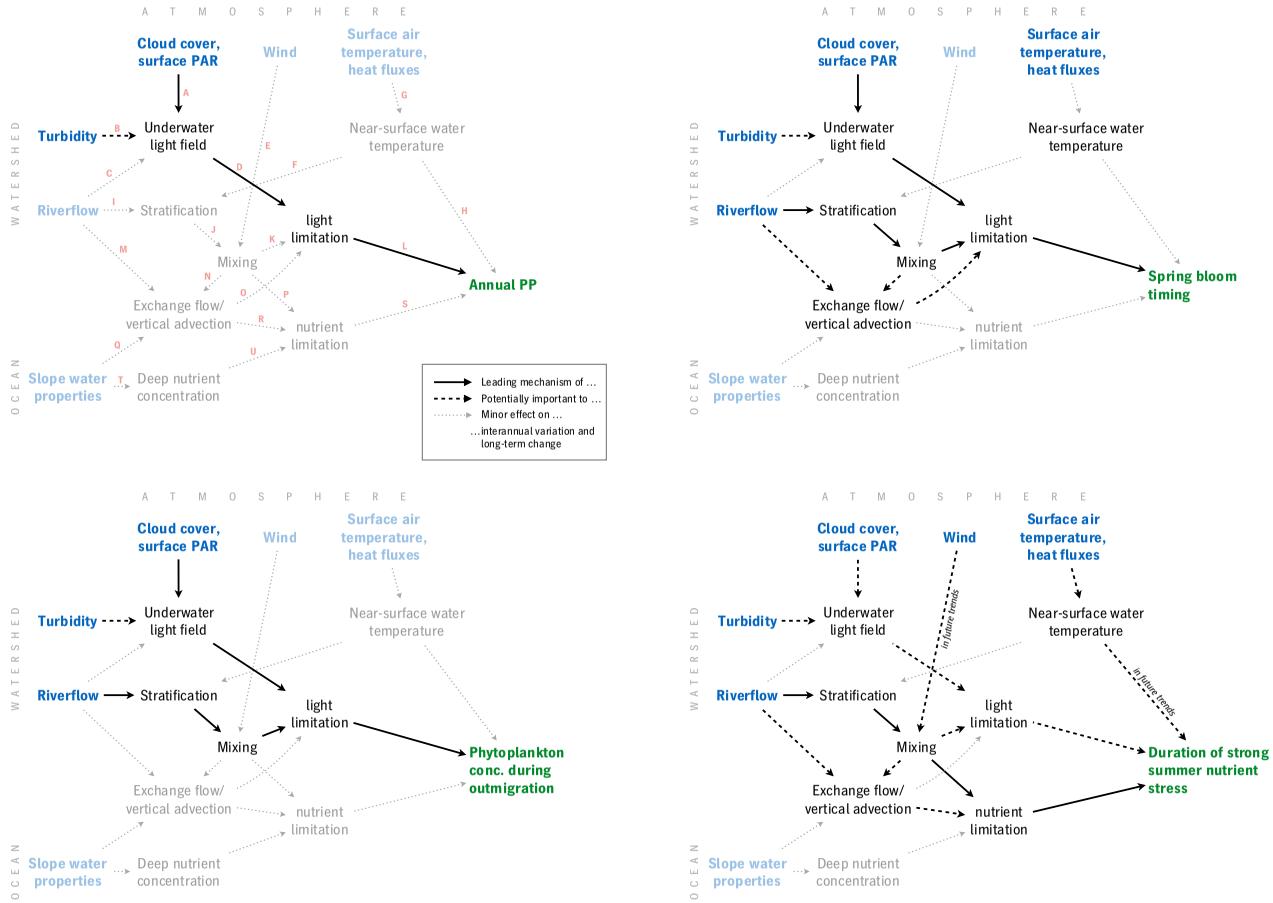

Figure 20: Final ranking of pathways of climate influence on four measures of phytoplankton dynamics.

Note that the PS-1D model does not include photoacclimation by individual cells, or succession of phytoplankton populations as environmental conditions change, and either mechanism would be expected to flatten out the response to variations in light conditions. Thus the sensitivity of PP_{tot} in our analysis is likely a high estimate.

Strikingly, variations in mixing and circulation have very small effects on PP_{tot} on interannual and longer timescales. This may be because changes in mixing have opposite effects in spring (via light) and summer (via nutrient supply), or because while turbulent mixing shows intense variation on short time and spatial scales, it is relatively steady in seasonal averages (2 s.d. $< 40\%$ variation, compared with around threefold variation over a typical tidal cycle). The other metrics in our analysis suggest the increased process complexity behind phytoplankton dynamics on event to seasonal scales, as opposed to annual averages.

4.2 Spring bloom timing

Variation in surface PAR (via variation in cloud cover) again emerges as a crucial influence on variation in spring bloom timing in central Main Basin (Table 7, Fig. 20). Historical variation in seasonally-averaged E_0 is sufficient to explain perhaps a 15 d range of spring bloom dates ($\pm$ 2 s.d.: Table 7), while event-(10 d) scale variation in E_0 is several times larger (Table 6) and leads to more than 2-month variation in t_{bloom} in PS-1D ($\pm$ 2 s.d.). The actual historical variation in t_{bloom} in Main Basin is unclear, since monthly DOE sampling could easily miss the bloom entirely and high-time-resolution ORCA chlorophyll time series are only available for a handful of years. However, the longer model-based estimate is close to the assessment by *Newton and Van Voorhis* (2002) (spring bloom March–May, 1999–2001) and also close to observed spring-bloom variability over 60 years in the southern Strait of Georgia.

The experiment in PS-1D that generated this estimate, in which we took event-scale variability in E_0, applied it over an entire annual cycle, and measured the change in spring bloom date, is mechanistically sensible enough if the spring bloom is a process with a short memory, a response to an event-scale confluence of suitable conditions. The SOG model predicts the southern Strait of Georgia spring bloom on the basis of Dec–Mar average conditions (*Collins et al.*, 2009; *Allen and Wolfe*, 2013); but there is no observational evidence that the Main Basin spring bloom is a response to seasonal-average conditions in this sense, and anecdotal evidence to the contrary (Fig. 15).

Allen and Wolfe (2013) found that variations in wind stress were as important a driver of spring bloom timing variability as variations in cloud cover and light, with temperature effects playing a secondary role. PS-1D shows a lower sensitivity of t_{bloom} to E_0 compared with SOG (-0.88 vs ~ 2 d $(\mathrm{W\ m^{-2}})^{-1}$), but also a lower sensitivity to temperature (1.5 vs. 4.7 d $(^\circ\mathrm{C})^{-1}$) and wind stress (20 vs. 70 d Pa^{-1}, Table 5). Accordingly, we find that wind mixing may have measurable effects on bloom date but appears to play a minor role compared with E_0, whereas riverflow-driven variation in stratification and mixing

has the same scale of effect as E_0 in seasonal averages. This ranking is consistent with the finding that in Main Basin, riverflow variability has stronger effects on mixing in spring than does wind stress (Table 6). Other than this, the minor differences in the ranking of controls on the spring bloom between our analysis and *Allen and Wolfe* (2013) appear to be driven mainly by differences in the phytoplankton models used (PS-1D vs. SOG), rather than differences between Main Basin and the southern Strait of Georgia as environments.

4.3 Conditions during salmon outmigration

We calculated variability in phytoplankton standing stock itself during the presumed period of juvenile steelhead and chinook outmigration and chinook outmigration, as an indication of possible changes in the light environment during a critical life stage for these fish. We speculate that the effect of a dense phytoplankton bloom on visual refuge and predation during this period would come through light scattering, not through light attenuation, and so we cannot directly compare the changes in the underwater light field that would result from the phytoplankton changes we model from the changes in light that drive the phytoplankton dynamics; however, this comparison would have to be made by studies that attempted to follow on from the results here. Overall, we find predicted changes in phytoplankton concentration, $P_{outmigr}^{steelhead}$ and $P_{outmigr}^{chinook}$, to be quite modest, on the order of 10% (Table 7). This might reflect the structural simplicity of PS-1D, or it might be an indication that if phytoplankton blooms have an effect on visual predation by and on juvenile salmoni, it is primarily through intense, transient, localised blooms, not through seasonal-average conditions. Surface PAR, underwater light, and (in the case of steelhead outmigration) riverflow effects on mixing drive the largest of these generally small effects.

4.4 Nutrient stress in summer

Although PS-1D does not resolve phytoplankton succession, the incidence of days in which nutrients become severely limiting can provide a clue to likely compositional changes during summer. Nutrient limitation under warm, high-light conditions has long been taken to encourage dinoflagellate blooms over diatoms, including toxin-producing taxa like *Alexandrium*; however, there is no detailed historical record in Puget Sound that supports a local link between nutrient limitation and *Alexandrium* HABs more directly. The metric Δt_{nut} counts the days in which surface NO3 + NH4 is less than 3 mmol m^{-3} in PS-1d, a threshhold that identifies an extreme but regularly occurring level of nutrient stress: its base-case value is 8 d per year.

Historical variation in seasonally-averaged surface PAR and in riverflow effects on stratification and mixing are both sufficient to drive variation in Δt_{nut} between approximately 0 and 2–3 times its base-case value (Table 7). Near-surface temperature and wind mixing do not appear likely to explain year-to-year variability but may well drive dramatic long-term trends (toward more

frequent or sustained nutrient stress in the case of temperature, and also toward higher nutrient stress if the prevailing northerly summer winds increase in strength: Table 7, *Moore et al.* (2015)). Changes in the exchange flow and background light attenuation could potentially also drive nutrient-stress changes of the same magnitude as the other mechanisms mentioned, but without a better quantification of seasonal-average patterns in these processes we cannot be sure.

For Δt_{nut} and to a lesser extent t_{bloom}, new temperature effects beyond the range of historical variability seem likely to emerge over the next few decades, if they have not already. Note that the effect of warming on nutrient stress in general, as discussed here, is likely accompanied by an independent effect of warming on *Alexandrium* growth rate and seasonal window of opportunity (*Moore et al.*, 2015).

5 Conclusion

The results of our multi-model synthesis and scaling analysis yield relatively simple pictures for interannual variation in primary production and phytoplankton standing stock in Main Basin (Fig. 20), in which a large number of potential pathways of climate influence can be classed as minor effects compared with others. Results paint more complex pictures for changes in the spring bloom date t_{bloom} and the count of days of strong nutrient stress in summer Δt_{nut}, both processes that involve event-scale changes atop seasonal changes. For these metrics, a large number of mechanistic pathways all seem capable of producing variations in phytoplankton dynamics on the same scale. This process complexity, and not just the incompleteness of available observations, may explain why simple correlative approaches to the Puget Sound spring bloom have never yielded a clear picture.

Overall, this study points to variation in incoming light, i.e. variation in cloud cover, as a leading climate influence on phytoplankton dynamics in Puget Sound. *Collins et al.* (2009) and *Allen and Wolfe* (2013) found the same for the timing of the spring bloom in the southern Strait of Georgia, although in that system (and the SOG model) wind mixing plays a comparable role, whereas in Puget Sound, riverflow effects on stratification and mixing exceed wind effects in spring (the two mechanisms are comparable in summer). (*Moore et al.*, 2015) previously suggested that long-term trends in Puget Sound hydrology, toward increased riverflow in spring and decreased flow in summer (*Cuo et al.*, 2009, 2011), might affect phytoplankton dynamics by modulating stratification and thus turbulent mixing. Our analysis of the relationship between riverflow and stratification (in historical observations) and stratification and mixing (in models) suggests that this pathway of influence likely drives significant interannual variation in phytoplankton dynamics as well, not just long-term trends, and in summer as well as spring.

Variations in light attenuation, beyond those explicable as phytoplankton self-shading, also appear to be intense enough to potentially drive important variability in primary production timing, magnitude, and nutrient limitation.

A simple approach to explaining this light-attenuation variablity in terms of salinity proved to be statistically weak; a more detailed investigation of what watershed characteristics link hydrology to the marine underwater light environment, and from there to effects on primary production, is clearly called for.

To some extent, this is exactly the kind of problem that regional earth system models have the potential to address, and a problem that might usefully serve as a nucleus for the next generation of coupled atmospheric-hydrologic-marine modelling in the Puget Sound basin. At the same time, the problem highlights gaps in our process understanding that can only be addressed through high-resolution observations and process studies, such as the role of plasticity and photoacclimation in modulating the response of the Puget Sound phytoplankton community to the light environment, and in setting the timing of the spring bloom. This need for broad and coordinated collaboration among modellers and observationalists of many stripes is likely a general characteristic of the long mechanistic chains that link climate variability and change to the dynamics of marine food webs.

Acknowledgements

This work was funded by Long Live the Kings, as part of the Salish Sea Marine Survival Project; the NOAA Monitoring and Event Response for Harmful Algal Blooms (MERHAB) program; Marine Alliance for Science and Technology Scotland (MASTS); and University of Strathclyde. Many thanks to Eric Salathé, Correigh Greene and Dave Beauchamp for their insights.

References

Allen, S. E., and M. A. Wolfe (2013), Hindcast of the timing of the spring phytoplankton bloom in the Strait of Georgia, 1968–2010, *Progress in Oceanography*, *115*(C), 6–13, doi:10.1016/j.pocean.2013.05.026.

Banas, N. S., L. Conway-Cranos, D. A. Sutherland, P. MacCready, P. Kiffney, and M. Plummer (2014), Patterns of River Influence and Connectivity Among Subbasins of Puget Sound, with Application to Bacterial and Nutrient Loading, *Estuaries and Coasts*, *38*(3), 735–753, doi:10.1007/s12237-014-9853-y.

Bissinger, J. E., D. Montagnes, J. Sharples, and D. Atkinson (2008), Predicting marine phytoplankton maximum growth rates from temperature: Improving on the Eppley curve using quantile regression, *Limnology and Oceanography*, *53*(2), 487–493.

Collins, A. K., S. E. Allen, and R. Pawlowicz (2009), The role of wind in determining the timing of the spring bloom in the Strait of Georgia, *Canadian Journal of Fisheries and Aquatic Sciences*, *66*(9), 1597–1616, doi:10.1139/F09-071.

Cuo, L., D. P. Lettenmaier, M. Alberti, and J. E. Richey (2009), Effects of a century of land cover and climate change on the hydrology of the Puget Sound basin, *Hydrological Processes*, *23*(6), 907–933, doi:10.1002/hyp.7228.

Cuo, L., T. K. Beyene, N. Voisin, F. Su, D. P. Lettenmaier, M. Alberti, and J. E. Richey (2011), Effects of mid-twenty-first century climate and land cover change on the hydrology of the Puget Sound basin, Washington, *Hydrological Processes*, *25*(11), 1729–1753, doi:10.1002/hyp.7932.

Davis, K. A., N. S. Banas, S. N. Giddings, S. A. Siedlecki, P. MacCready, E. J. Lessard, R. M. Kudela, and B. M. Hickey (2014), Estuary-enhanced upwelling of marine nutrients fuels coastal productivity in the U.S. Pacific Northwest, *Journal of Geophysical Research*, *119*(12), 8778–8799, doi:10.1002/2014JC010248.

Dulière, V., Y. Zhang, and E. P. Salathé Jr (2011), Extreme precipitation and temperature over the us pacific northwest: A comparison between observations, reanalysis data, and regional models, *Journal of Climate*, *24*(7), 1950–1964.

Eppley, R. W. (1972), Temperature and phytoplankton growth in the sea, *Fishery Bulletin*, *70*(4), 1063–1085.

Franks, P. J. S. (2015), Has Sverdrup's critical depth hypothesis been tested? Mixed layers vs. turbulent layers, *ICES Journal of Marine Science*, *72*(6), 1897–1907, doi:10.1093/icesjms/fsu175.

Giddings, S. N., P. MacCready, B. M. Hickey, N. S. Banas, K. A. Davis, S. A. Siedlecki, V. L. Trainer, R. M. Kudela, N. A. Pelland, and T. P. Connolly (2014), Hindcasts of potential harmful algal bloom transport pathways on the Pacific Northwest coast, *J. Geophys. Res.*, doi:10.1002/2013JC009622.

Horner, R. A., C. L. Greengrove, K. S. Davies-Vollum, J. E. Gawel, J. R. Postel, and A. M. Cox (2011), Spatial distribution of benthic cysts of Alexandrium catenella in surface sediments of Puget Sound, Washington, USA, *Harmful Algae*, *11*, 96–105, doi:10.1016/j.hal.2011.08.004.

Khangaonkar, T., A. Nugraha, W. Xu, and K. Balaguru (2019), Salish Sea Response to Global Climate Change, Sea Level Rise, and Future Nutrient Loads, *Journal of Geophysical Research: Oceans*, pp. 2018JC014,670–72, doi:10.1029/2018JC014670.

Large, W. G., and S. Pond (1981), Open ocean momentum flux measurements in moderate to strong winds, *Journal of Physical Oceanography*, *11*(3), 324–336, doi:10.1175/1520-0485(1981)011¡0324:OOMFMI¿2.0.CO;2.

Mackas, D. L., and P. J. Harrison (1997), Nitrogenous nutrient sources and sinks in the juan de fuca strait/strait of georgia/puget sound estuarine system: assessing the potential for eutrophication, *Estuarine, Coastal and Shelf Science*, *44*(1), 1–21.

McGillicuddy, J., DJ, D. W. Townsend, R. He, B. A. Keafer, J. L. Kleindinst, Y. Li, J. P. Manning, D. G. Mountain, M. A. Thomas, and D. M. Anderson (2011), Suppression of the 2010 alexandrium fundyense bloom by changes in physical, biological, and chemical properties of the gulf of maine, *Limnology and Oceanography*, *56*(6), 2411–2426.

Mohamedali, T., M. Roberts, B. Sackmann, and A. Kolosseus (2011), Puget sound dissolved oxygen model nutrient load summary for 1999–2008, *Lacey: Washington State Department of Ecology, Publication*, (11-03), 057.

Moore, S. K., N. J. Mantua, and E. P. Salathé Jr (2011), Past trends and future scenarios for environmental conditions favoring the accumulation of paralytic shellfish toxins in Puget Sound shellfish, *Harmful Algae*, *10*(5), 521–529.

Moore, S. K., J. A. Johnstone, N. S. Banas, and E. P. Salathé Jr (2015), Present-day and future climate pathways affecting Alexandrium blooms in Puget Sound, WA, USA, *Harmful Algae*, *48*, 1–11, doi:10.1016/j.hal.2015.06.008.

Newton, J. A., and K. Van Voorhis (2002), Seasonal Patterns and Controlling Factors of Primary Production in Puget Sound's Central Basin and Possession Sound, *Tech. rep.*, Washington State Department of Ecology.

Newton, J. A., E. Siegel, and S. L. Albertson (2003), Oceanographic changes in Puget Sound and the Strait of Juan de Fuca during the 2000-01 drought, *Canadian Water Resources Journal*, *28*(4), 715–728.

Nguyen, H. T. T. (2020), Biogeochemical modelling of fjord and sea lochs, Ph.D. thesis, University of Strathclyde, in preparation.

Poli, R., J. Kennedy, and T. Blackwell (2007), Particle swarm optimization, *Swarm Intelligence*, *1*(1), 33–57, doi:10.1007/s11721-007-0002-0.

Shannon, J. G. (1975), Correlation Of Beam And Diffuse Attenuation Coefficients Measured In Selected Ocean Waters, in *Ocean Optics IV*, vol. 0064, pp. 3 – 11, International Society for Optics and Photonics, SPIE, doi:10.1117/12.954489.

Siedlecki, S. A., N. S. Banas, K. A. Davis, S. Giddings, B. M. Hickey, P. MacCready, T. Connolly, and S. Geier (2015), Seasonal and interannual oxygen variability on the Washington and Oregon continental shelves, *Journal of Geophysical Research: Oceans*, doi:10.1002/2014JC010254.

Smith, S. L., Y. Yamanaka, M. Pahlow, and A. Oschlies (2009), Optimal uptake kinetics: physiological acclimation explains the pattern of nitrate uptake by phytoplankton in the ocean, *Marine Ecology Progress Series*, *384*, 1–13, doi:10.3354/meps08022.

Stone, H. B., N. S. Banas, and P. MacCready (2018), The Effect of Alongcoast Advection on Pacific Northwest Shelf and Slope Water Properties in Relation to Upwelling Variability, *Journal of Geophysical Research: Oceans*, *123*(1), 265–286, doi:10.1002/2017JC013174.

826 Sutherland, D. A., P. MacCready, N. S. Banas, and L. F. Smedstad (2011),
827 A Model Study of the Salish Sea Estuarine Circulation, *Journal of Physical*
828 *Oceanography*, *41*(6), 1125–1143, doi:10.1175/2011JPO4540.1.

829 Wan, H., X. L. Wang, and V. R. Swail (2010), Homogenization and trend anal-
830 ysis of canadian near-surface wind speeds, *Journal of Climate*, *23*(5), 1209–
831 1225, doi:10.1175/2009JCLI3200.1.

832 Winter, D. F., G. C. Anderson, and K. Banse (1975), The Dynamics of Phyto-
833 plankton Blooms in Puget Sound, a Fjord in the Northwestern United States.

834 Zimmerman, M. S., J. R. Irvine, M. O'Neill, J. H. Anderson, C. M. Greene,
835 J. Weinheimer, M. Trudel, and K. Rawson (2015), Spatial and Tem-
836 poral Patterns in Smolt Survival of Wild and Hatchery Coho Salmon
837 in the Salish Sea, *Marine and Coastal Fisheries*, *7*(1), 116–134, doi:
838 10.1080/19425120.2015.1012246.